Article

Rewiring cancer drivers to activate apoptosis

https://doi.org/10.1038/s41586-023-06348-2

Received: 15 August 2022

Accepted: 20 June 2023

Published online: 26 July 2023

Check for updates

Sai Gourisankar[1,2,6], Andrey Krokhotin[1,6], Wenzhi Ji[3,6], Xiaofan Liu[3], Chiung-Ying Chang[1], Samuel H. Kim[1], Zhengnian Li[3], Wendy Wenderski[1,4], Juste M. Simanauskaite[1], Haopeng Yang[5], Hannes Vogel[1], Tinghu Zhang[3], Michael R. Green[5], Nathanael S. Gray[3]✉ & Gerald R. Crabtree[1,4]✉

Genes that drive the proliferation, survival, invasion and metastasis of malignant cells have been identified for many human cancers[1–4]. Independent studies have identified cell death pathways that eliminate cells for the good of the organism[5,6]. The coexistence of cell death pathways with driver mutations suggests that the cancer driver could be rewired to activate cell death using chemical inducers of proximity (CIPs). Here we describe a new class of molecules called transcriptional/epigenetic CIPs (TCIPs) that recruit the endogenous cancer driver, or a downstream transcription factor, to the promoters of cell death genes, thereby activating their expression. We focused on diffuse large B cell lymphoma, in which the transcription factor B cell lymphoma 6 (BCL6) is deregulated[7]. BCL6 binds to the promoters of cell death genes and epigenetically suppresses their expression[8]. We produced TCIPs by covalently linking small molecules that bind BCL6 to those that bind to transcriptional activators that contribute to the oncogenic program, such as BRD4. The most potent molecule, TCIP1, increases binding of BRD4 by 50% over genomic BCL6-binding sites to produce transcriptional elongation at pro-apoptotic target genes within 15 min, while reducing binding of BRD4 over enhancers by only 10%, reflecting a gain-of-function mechanism. TCIP1 kills diffuse large B cell lymphoma cell lines, including chemotherapy-resistant, *TP53*-mutant lines, at EC_{50} of 1–10 nM in 72 h and exhibits cell-specific and tissue-specific effects, capturing the combinatorial specificity inherent to transcription. The TCIP concept also has therapeutic applications in regulating the expression of genes for regenerative medicine and developmental disorders.

Induced proximity is fundamental to many forms of biological regulation, including receptor function[9], post-translational modifications[10,11], regulation of transcription[12,13], epigenetic regulation[14–16] and allosteric processes that generate scaffolds to facilitate protein–protein interactions. The underlying physical principle is based on the fact that an effective collision between two molecules is inversely proportional to the cube of the distance between them[15]. The biological roles of induced proximity have been probed with dimeric small molecules, CIPs, that have been used to recapitulate many steps in signal transduction, protein localization and transcription[15]. Recently, dimeric small molecules that use CIP to target proteins to the proteasome, PROTACS[17], or to inhibit protein–protein interactions[18] have been developed. More broadly, the observation that even an event as carefully regulated as programmed cell death can be activated by CIPs[19–21] suggests that distinct cellular circuitries might be linked, or rewired, using CIPs, to cause cancer cells to activate processes leading to apoptosis.

To rewire transcriptional circuits within a genetically unmodified cell or organism, we developed small molecules that allow the recruitment of cancer-driving transcriptional or epigenetic regulators to the regulatory regions of target therapeutic genes. The general features of the concept and design of a TCIP is illustrated in Fig. 1a and involves synthesis of small molecules that bind to a specific transcriptional or epigenetic regulator on one side; on the other side, a transcription factor binds to a target therapeutic gene. We applied these molecules to activate apoptosis in cancer cells.

TCIP1 selectively kills DLBCL cells

To design the first TCIPs, we targeted diffuse large B cell lymphoma (DLBCL) and made use of small molecules that bind to the BTB domain of BCL6 and inhibit its interaction with nuclear receptor corepressor (NCOR), BCL6 corepressor (BCOR) and silencing mediator of retinoic acid and thyroid hormone receptor (SMRT), which epigenetically suppress some BCL6 targets including pro-apoptotic, cell cycle arrest and DNA-damage response genes[22], such as *TP53* (ref. 8) (Fig. 1b). To provide additional transcriptional activation of pro-apoptotic genes,

[1]Department of Pathology, Stanford University, Stanford, CA, USA. [2]Department of Chemical Engineering, Stanford University, Stanford, CA, USA. [3]Department of Chemical and Systems Biology, Stanford Cancer Institute, ChEM-H, Stanford University, Stanford, CA, USA. [4]Department of Developmental Biology, Stanford University, Stanford, CA, USA. [5]Department of Lymphoma & Myeloma, The University of Texas MD Anderson Cancer Center, Houston, TX, USA. [6]These authors contributed equally: Sai Gourisankar, Andrey Krokhotin, Wenzhi Ji. ✉e-mail: nsgray01@stanford.edu; crabtree@stanford.edu

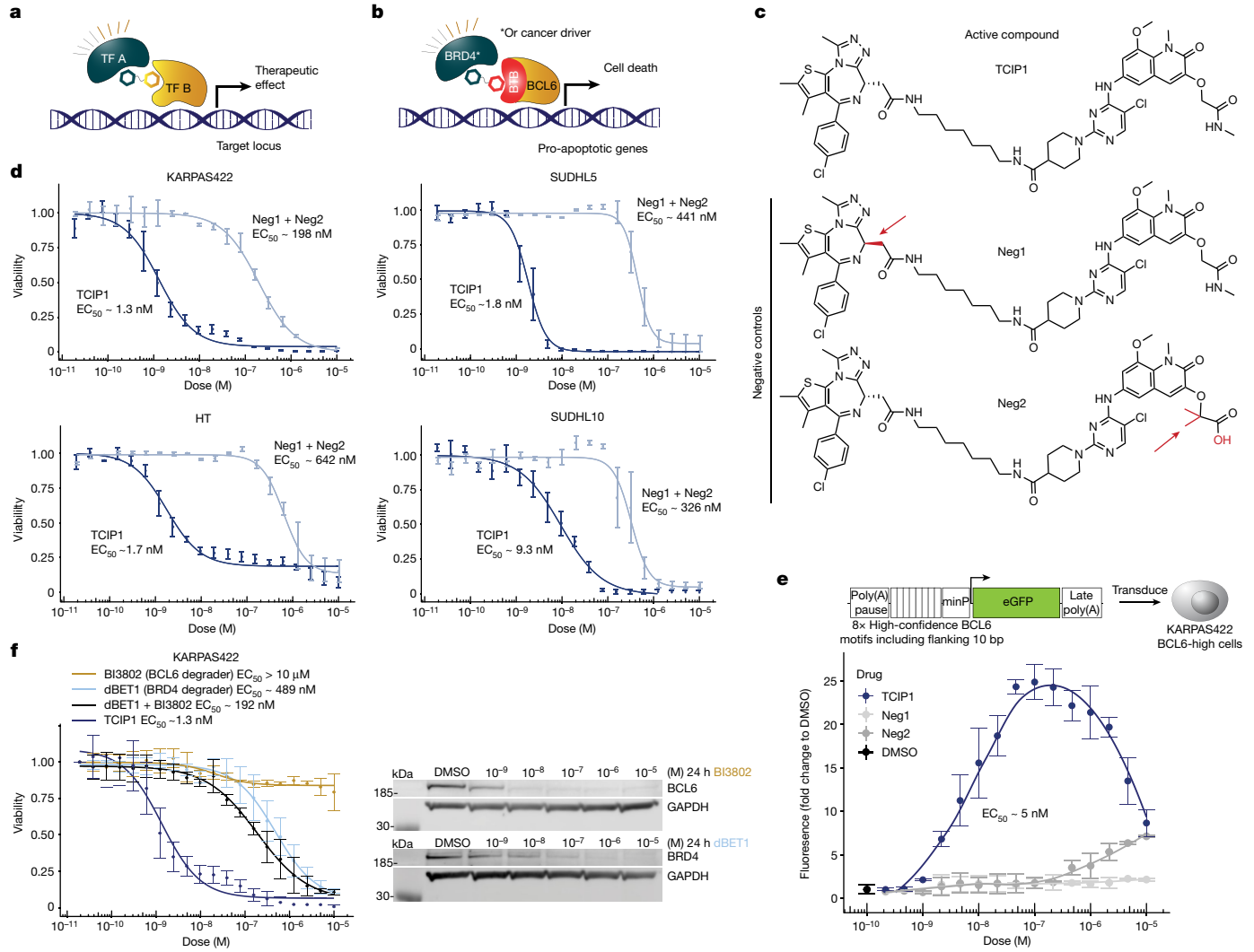

Fig. 1 | Production of TCIPs. a, An endogenous target gene is activated or repressed using a bivalent molecule binding one endogenous transcription factor (TF) or epigenetic regulator on one side, chemically linked to a moiety that binds to a second transcription factor that binds to the regulatory region of a target gene, which might induce production of a therapeutic gene. **b**, A specific TCIP that recruits a transcriptional activator (BRD4) or cancer driver to the BCL6 repressor on cell death genes, thereby derepressing transcription and inducing transcription driven by BCL6. **c**, Chemical structures of the most potent BCL6–BRD4 TCIP, TCIP1 and the negative controls Neg1 (BRD4 non-binding) and Neg2 (BCL6 non-binding). **d**, TCIP1 effect on cell viability of the chemotherapy-resistant, *TP53*-mutant DLBCL cell line KARPAS422, as well as three other DLBCL cell lines with high levels of BCL6. $n = 4$ biological replicates, mean ± s.d. **e**, Design and activation of a BCL6 reporter with TCIP1 in KARPAS422 cells at 8 h after drug addition. $n = 4$ biological replicates, mean ± s.d. minP, minimal promoter. **f**, Comparison of TCIP1 effect on cell viability with the effect of BRD4 or BCL6 degraders ($n = 3$ biological replicates, mean ± s.d). Viability curves in **d** and **f** are after 72 h of drug treatment.

over simple derepression, we covalently linked one such BTB binder, BI3812 (ref. 23), covalently to the bromodomain and extraterminal (BET) protein family binder JQ1 (ref. 24), which binds comparably to both bromodomains of BRD4 and slightly less potently to the bromodomains of BRD2 and BRD3 (Fig. 1c). These bromodomain proteins are involved in transcription and contribute a driving function to several tumours by facilitating MYC activation[25].

These molecules were tested for their effect on viability of the chemotherapy-resistant DLBCL cell line KARPAS422. This line has biallelic inactivation of *TP53* and was chosen for its high level of expression of BCL6 and the fact that it has multiple cancer drivers[26,27]. TCIP1 rapidly and robustly killed KARPAS422 with a half-maximal effective concentration (EC_{50}) of 1.3 nM, 72 h after the addition of drug (Fig. 1d). Three other DLBCL lines with high levels of BCL6 (Fig. 1d) were also rapidly and robustly killed by TCIP1. Adding JQ1 and BI3812 separately or together showed 100–1,000-fold less-effective cell killing (Extended Data Fig. 1a), excluding the possibility that TCIP1 acts by simply delivering two inhibitors into the cell. We synthesized negative chemical controls—Neg1 and Neg2—with the same linker structure as TCIP1 but with modifications known to mitigate binding to BRD4 or BCL6, respectively[23,24]. Neg1 and Neg2 had greater than 100-fold less effect on cell viability than did TCIP1, even in combination (Fig. 1d), suggesting that binding both proteins in proximity is required for effective killing. We noted that unlike TCIP1, both BI3812 and JQ1 left a substantial resistant population of cells alive, as has been previously reported[28].

In a panel of 14 lymphoma and other blood cancer cell lines, killing, as measured by EC_{50}, correlated with BCL6 levels (Extended Data Fig. 1b). Some DLBCL cell lines such as OCILY19, with no detectable level of BCL6 (Extended Data Fig. 1b), showed little or no response compared with controls. The level of expression of BCOR, NCOR and SMRT varied among the cell lines and could also contribute to the variation in sensitivity[29]. Among the cell lines tested, there was no evidence that killing required TP53, nor was there evidence of repression of killing by endogenous BCL2 levels (Extended Data Fig. 1b,c). To examine the

potency of TCIP1 among diverse cancer types, we carried out an unbiased screen of the effect of TCIP1 on the viability of 906 cancer cell lines (PRISM[30]) originating from various lineages. The most sensitive cancer cells were those that both originated from haematopoietic and/or lymphoid tissues and had high BCL6 levels (Extended Data Fig. 1d).

To test whether TCIP1 derepresses BCL6-regulated gene expression using endogenous levels of BCL6 and BRD4, we designed a BCL6 reporter from known BCL6-binding sites at promoters of cell death genes such as *TP53* and *CASP8*, based on BCL6 chromatin immunoprecipitation followed by sequencing (ChIP–seq) data in DLBCL cells, including the flanking 10 bp to capture any co-binding of endogenous transcription factors (Fig. 1e). Addition of TCIP1 revealed dose-dependent activation at 8 h, with an EC_{50} of 5 nM, similar to the EC_{50} of cell viability in these cells (Fig. 1d). Reporter activation also featured a characteristic 'hook effect', reflecting competition among bivalent molecules for limited endogenous proteins, and the controls Neg1 and Neg2 did not activate the reporter. We also noted that TCIP1 was 200–10,000-fold more potent in killing DLBCL cells than was degradation of BRD4 by dBET1 (ref. 31) and/or degradation of BCL6 by BI3802 (ref. 32) (Fig. 1f), indicating that simple sequestration of these proteins is not the primary contributor to the potency of TCIP1.

Cell killing requires a ternary complex

The 1,000-fold increase in potency of TCIP1 over BRD4 or BCL6 degradation suggested the formation of a gain-of-function ternary complex between BRD4, BCL6 and TCIP1. We carried out chemical rescue experiments in which we titrated increasing concentrations of either JQ1 or BI3812 to multiple DLBCL cell lines, against constant concentrations of TCIP1 that kill 50–95% of cells within 72 h. JQ1 or BI3812 prevented death by TCIP1, indicating that both the BRD4-binding and the BCL6-binding side of TCIP1 are essential for effective killing (Fig. 2a,b). Examination of other DLBCL lines indicated that death of cell lines with little or no BCL6 could not be rescued (Extended Data Fig. 2a–c), and that in cell lines with low levels of BCL6, the potency of TCIP1 was comparable with Neg2, suggesting that the effects of TCIP1 in lines without BCL6 are due to simple BRD4 inhibition (Extended Data Fig. 2d,e).

To quantify the direct interaction between TCIP1, BRD4 and BCL6, we developed a time-resolved fluorescence resonance energy transfer (TR-FRET) assay based on the proximity of the BTB domain of BCL6 labelled with fluorescein isothiocyanate (FITC) to bromodomain 1 (BD1) of BRD4 detected with an anti-histidine tag, terbium-conjugated antibody (Fig. 2c). Formation of a ternary complex in vitro, related to TR-FRET peak height and area under the curve[33], was detected using TCIP1 as well as multiple TCIP molecules shown in Fig. 2e.

One reason for the broad hook effect observed in the TR-FRET assay for TCIP1 and other potent TCIPs (Fig. 2c,e and Extended Data Fig. 3a) is the formation of cooperative protein–protein interactions induced by the drug, such as a molecular glue[9,34,35]. To examine this in detail, we carried out isothermal calorimetry binary and ternary titrations of TCIP1, BRD4(BD1) and BCL6(BTB). Both binary interactions of BCL6–TCIP1 and BRD4–TCIP1 were weak (K_d of BRD4–TCIP1 = 5.08 μM; K_d of BCL6–TCIP1 > 1 mM; Extended Data Fig. 3b), but the ternary complex affinity was K_d of BRD4–TCIP1–BCL6 = 340 ± 108 nM (mean ± s.d., $n = 3$) (Fig. 2d, left). Using an orthogonal method, biolayer interferometry, we obtained a similar affinity of K_d of BRD4–TCIP1–BCL6 = 293 ± 132 nM (Fig. 2d, right) and confirmed the weak interaction between TCIP1 and BCL6(BTB). We verified the published affinities of JQ1 to BRD4(BD1) and BI3812 to BCL6(BTB), and also that the protein domains do not interact on their own (Extended Data Fig. 3b). Biolayer interferometry measurements also revealed that the ternary complex has a slow off-rate of 26 ms^{-1} with a half-life of 30 s (Extended Data Fig. 3c–e). Together, the data indicate that TCIP1 induces a stable, cooperative protein–protein interaction between bromodomain 1 of BRD4 and the BTB domain of BCL6.

TCIP1 was the most potent in cell killing among a small library of related TCIPs using different linkers (Fig. 2e). To better understand the relationship between the molecular structure and cellular activity of TCIP, we analysed the relationship between BCL6 reporter transactivation in DLBCL cells and favourable ternary complex formation in vitro and inside the cell (Fig. 2f,g). The most potent TCIPs at cell killing and activating the BCL6 reporter also had high affinities of in vitro and intracellular ternary complex formation (Fig. 2f,g and Extended Data Fig. 3f). The data are consistent with the requirement of an intracellular ternary complex of BRD4, TCIP1 and BCL6 for the activation of cell death.

Apoptosis throughout the cell cycle

To characterize the cell death observed with TCIP1, we quantified cells that have externalized phosphatidylserine by staining with annexin V. We observed a dose-dependent increase in the number of annexin-positive cells, at 10 nM TCIP1, at 24 h (Extended Data Fig. 4a). TCIP1 induced detectable apoptosis by 4–8 h (Extended Data Fig. 4b).

Cancers can evade cell killing by many chemotherapeutics that function only during a specific stage of the cell cycle. To investigate the cell-cycle dependence of the apoptosis caused by TCIP1, we performed cell-cycle analysis in concert with TUNEL staining, which measures DNA fragmentation (Extended Data Fig. 4c). The cell-cycle analysis revealed that TCIP1 induced both a G1/S and G2/M block in the cell cycle (Extended Data Figs. 4d and 5a). By examining DNA cleavage with the TUNEL assay, we found that cell death occurred during all phases of the cell cycle (Extended Data Figs. 4e and 5a). To further examine the mechanism of cell death by TCIP1, we used serum starvation to arrest the cell cycle in G0/G1. The cells became even more sensitive to TCIP1, exhibiting an EC_{50} of 250 pM compared with 3.2 nM without arrest (Extended Data Fig. 4f). This observation indicates that TCIP1 produces cell death by activating more than a single cell death pathway.

TCIP1 activates pro-apoptotic genes

To define the genes involved in the induction of apoptosis by TCIP1, we carried out RNA sequencing studies 20 h after adding drug at 10 or 100 nM, when the critical genes were likely to be executing their functions. Changes in gene expression were dependent on dose (Extended Data Fig. 6a–c), and at just 10 nM TCIP1, the expression of 1,654 genes was increased, whereas the expression of 1,347 genes was reduced (Fig. 3a). Genes activated by TCIP1 were enriched for known cell-cycle arrest and pro-apoptotic targets normally repressed by BCL6, such as *P21* (also known as *CDKN1A*), *FOXO3* and *PMAIP1* (also known as *NOXA*) (Fig. 3a and Extended Data Fig. 6b,c,e). Along with the p53 and apoptosis pathways, TCIP1 also induces the TNF pathway (Extended Data Fig. 6d). Signalling via NF-κB has been shown to be repressed by BCL6 (refs. 22,36,37). These changes in mRNA levels were paralleled by dose-dependent and time-dependent changes in protein expression in two different DLBCL cell lines, SUDHL5 and KARPAS422, with negligible effect of the chemical controls Neg1 and Neg2 (Fig. 3d–f). Of particular interest was the observation that *FOXO3* is activated by 0.5 nM TCIP1 (Fig. 3e) and within 2 h by 10 nM TCIP1 (Fig. 4d). Activation of *FOXO3* also displayed a hook effect (Fig. 3e), characteristic of the direct target of a bivalent molecule. *FOXO3* is a master pro-apoptotic gene[38] with a BCL6-binding site at its promoter[39]. Although *FOXO3* and *P21* are also known to be activated downstream of *TP53* (ref. 40), which is itself a BCL6 target, *TP53* is biallelically inactivated in this DLBCL line (KARPAS422) and other chemotherapy-resistant DLBCL lines killed by TCIP1. This supports the evidence in Extended Data Fig. 4 that TCIP1 derepresses multiple cell-cycle arrest and death pathways that are normally repressed by BCL6.

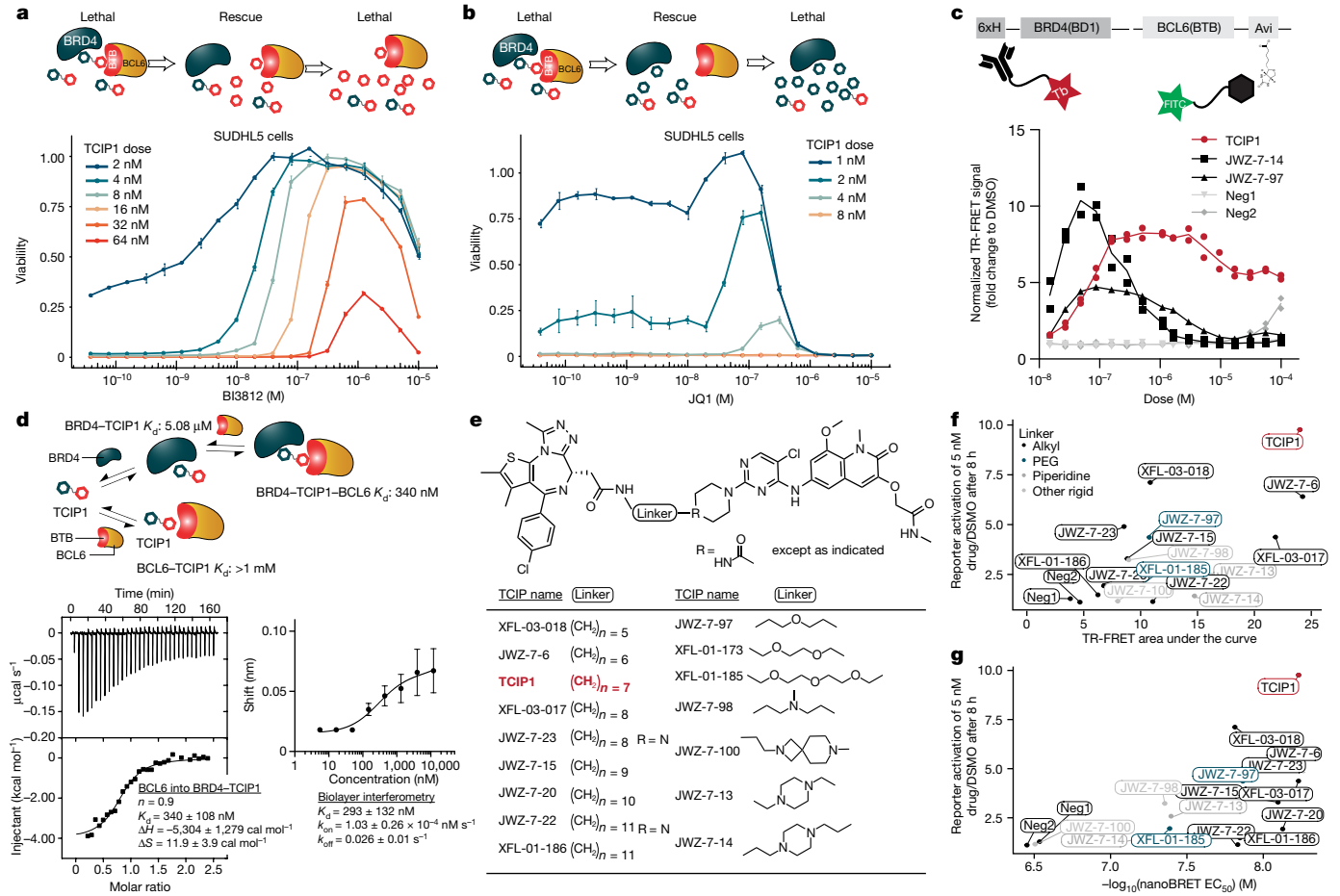

Fig. 2 | TCIP1 functions by inducing ternary complex formation. **a**, Competitive titration of BI3812 against TCIP1. TCIP1 was added at concentrations from 2 to 64 nM that killed 90% of SUDHL5 DLBCL cells at the same time as addition of the indicated concentrations of BI3812. $n = 3$ biological replicates, mean ± s.d., 72 h of drug treatment. **b**, Competitive titration of JQ1 against TCIP1. $n = 3$ biological replicates, mean ± s.d, 72 h of drug treatment. **c**, TR-FRET assay to measure molecule-dependent ternary complex formation between BRD4(BD1) and BCL6(BTB). Plotted are a representative set of TCIPs that were the most potent (in cell viability assays) within each category of linker structure. TCIP1 had the highest potency of all designed molecules. Each point represents an independent replicate, which is the mean of three technical repeats; the mean value line is drawn. **d**, Analysis of cooperative binding induced by TCIP1 and the BRD4(BD1) and BCL6(BTB) domains. A representative ternary complex K_d measurement by isothermal calorimetry is shown. For binary measurements, see Extended Data Fig. 3b. $n = 3$ independent replicates, mean ± s.d. Isothermal calorimetry parameters shown are 20:1 BRD4(BD1):TCIP1 in the cell and titration of BCL6(BTB). For biolayer interferometry, measurements were with 50 µM excess BRD4(BD1) in the well, nanomolar titrations of TCIP1 and biotinylated BCL6(BTB) on the tip. $n = 3$ independent replicates. The points and error bars are mean ± s.e. The K_d value is mean ± s.d. ΔH, enthalpy; ΔS, entropy; k_{on}, on-rate of binding; k_{off}, off-rate of binding. **e**, Multiple BRD4–BCL6 TCIPs synthesized with different linkers to test the structure–activity relationship. **f**, Effect of favourable in vitro ternary complex formation (represented by TR-FRET area under the curve) on the transcriptional activation of the BCL6 reporter in DLBCL cells. **g**, Effect of favourable intracellular ternary complex formation (represented by nanoBRET EC_{50}) on the transcriptional activation of the BCL6 reporter in DLBCL cells.

TCIP1 represses MYC and its targets

Among the group of genes whose expression was most reduced were *MYC* and its targets (Fig. 3b and Extended Data Fig. 6c). This is important as many DLBCLs are considered to be dependent on MYC[41,42]. We examined the top 100 most TCIP1-reduced genes using over 4,500 ChIP–seq datasets of human transcription factors in blood cancer cell lines[43], and found the promoters of TCIP1-inhibited genes highly enriched for MYC binding in multiple datasets (Fig. 3c). Examination of MYC protein levels upon the addition of TCIP1 showed that MYC levels were reduced starting at less than 1 nM TCIP1 and within 2 h of addition of the drug (Fig. 3d,e). The chemical controls Neg1 and Neg2 did not affect MYC levels at comparable concentrations (Fig. 3f). BET/BRD4 inhibitors such as JQ1 are known to reduce the expression of MYC[25], but at much higher levels of drug (500 nM) than TCIP1. We therefore hypothesized that repression of MYC is a gain-of-function consequence of the ternary complex formed by TCIP1.

To clarify the role of ternary complex formation for the repression of MYC as well as other gene expression and protein level changes observed, we blocked binding of TCIP1 to BCL6 by titrating the BCL6(BTB) inhibitor BI3812 against a constant concentration of 10 nM TCIP1 (Fig. 3g). Titration of BI3812 prevented downregulation of MYC, as well as reversed upregulation of p21 and FOXO3 (Fig. 3g). The results indicate that both activation of pro-apoptotic targets and repression of MYC are mediated by the formation of a ternary complex between BRD4, TCIP1 and BCL6, and support the evidence in Fig. 2 that the active biological entity is the ternary complex.

Identification of direct targets of TCIP1

The addition of 10 nM TCIP1 to KARPAS422 cells for 1, 2 and 4 h and subsequent measurement of RNA identified a selective set of approximately 140 genes induced by TCIP1, including well-characterized BCL6-repressed targets such as the apoptotic regulators *BCL2L11* (also

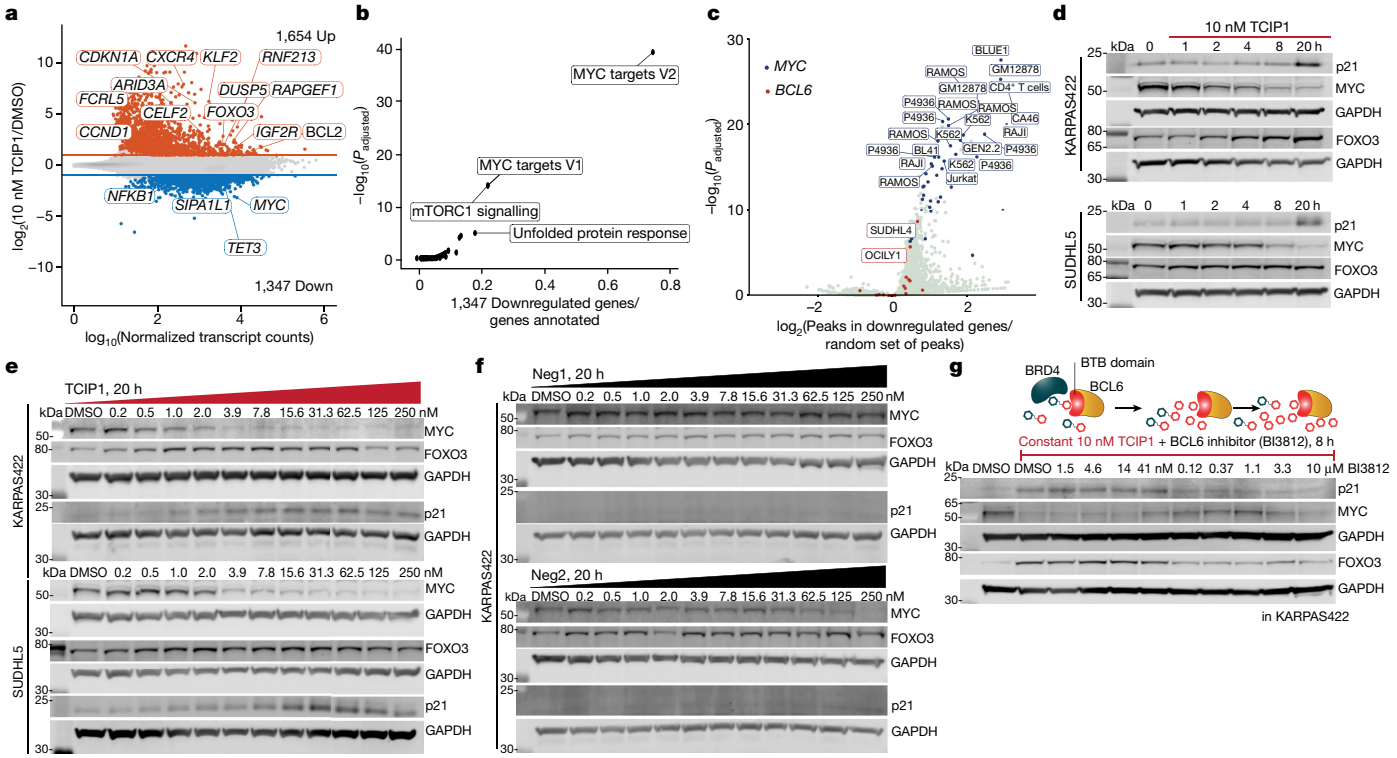

Fig. 3 | TCIP1 represses MYC and its targets while activating pro-apoptotic genes. a, Gene activation (median change: fourfold up) and repression after addition of 10 nM TCIP1 in KARPAS422 cells for 20 h, with well-known BCL6 targets labelled. Significance cut-offs were $P_{adjusted} \leq 0.05$ and $|\log_2(\text{drug/DMSO})| \geq 1$); $n = 2$ biological replicates. **b**, Downregulated genes are significantly enriched for MYC targets (MSigDB hallmark pathways). **c**, Analysis of transcription factor binding of the top 100 downregulated genes in 4,500 or more public ChIP–seq datasets in blood-lineage cells. For **b**,**c**, the adjusted *P* values were computed by two-sided Fisher's exact test and adjusted for multiple comparisons by Benjamini–Hochberg. **d**, Kinetics of protein changes in MYC, p21 and FOXO3 in DLBCL cell lines after treatment with 10 nM TCIP1. **e**, Dose-dependent changes in protein levels of target genes selected from the RNA sequencing results in two separate DLBCL cell lines, KARPAS422 and SUDHL5. **f**, Negligible effect of the negative controls Neg1 and Neg2 on protein levels of TCIP1 targets. For **d**–**f**, blots are representative of two biological replicates, except KARPAS422 in **d** and in **e** where data represent three biological replicates. **g**, Rescue of p21 and FOXO3 upregulation and MYC downregulation by competitive titration of the BTB binder BI3812 against constant 10 nM TCIP1 treatment for 8 h. Representative of two biological replicates. In all blots in **d**–**g**, any markers immunoblotted for the same gel are followed immediately by the loading control GAPDH run on that same gel.

known as *BIM*)[44], *PMAIP1*, *FOXO3* and *BCL6*. These probably represent direct transcriptional targets of TCIP1 (Fig. 4a). Almost all differential genes were increasingly activated at 1, 2 and 4 h, compared with negligible effects of the control molecules Neg1 and Neg2 (Fig. 4b). BCL6-repressed pathways such as TNF signalling and p53 pathways began to be upregulated at 1 and 2 h, and *MYC* targets only began to be repressed at 4 h (Extended Data Fig. 7c), consistent with reduction of MYC protein levels after 2 h (Fig. 3d). Although several genes showed reduced expression in TCIP1-treated cells at the early 1 and 2 h timepoints, in contrast to the upregulated genes, they were not statistically significantly enriched for any particular biological pathway (Extended Data Fig. 7c) and could represent general stress from the onset of DNA fragmentation. Analysis of BCL6 occupancy at promoters of upregulated genes, using published BCL6 ChIP–seq in the DLBCL line OCILY1 (ref. 39), showed that 53%, 57% and 55%, respectively, of upregulated genes at 1, 2 and 4 h had high-confidence BCL6 peaks within 1 kb of their transcription start site (see Methods). Further analysis using over 4,500 ChIP–seq datasets of various human transcription factors in blood cancer cell lines[43] revealed that the promoters of TCIP1-activated genes were statistically significantly enriched for BCL6 binding in multiple datasets (Fig. 4c). These studies indicate that TCIP1 specifically activates BCL6 target genes.

ChIP–seq studies of BRD4 after 1 h of drug addition revealed that TCIP1 produced a consistent, modest approximately 1.5-fold increase in BRD4 recruitment to BCL6 sites over the genome (Fig. 4d). This observation could indicate that TCIP1 needs to recruit only small amounts of BRD4 to produce the robust activation of BCL6 targets observed, and/or that the two other BET proteins expressed in these cells, BRD2 and BRD3, also mediate its effects. BRD4 and other BET proteins have previously been implicated largely in transcriptional elongation, particularly in mediating activation of RNA polymerase II (Pol II) elongation activity by phosphorylation of serine 2 of its C-terminal domain (CTD) (Pol II Ser2 phos)[45]. The other major CTD modification of Pol II is serine 5 phosphorylation (Pol II Ser5 phos), which marks paused polymerase ready to initiate transcription[46]. These serines are actively phosphorylated and dephosphorylated during the cycle of transcription. To closely examine the consequences of the addition of TCIP1 on transcription, we carried out short timepoint ChIP–seq experiments with antibodies specific to these CTD modifications as well as acetylation of lysine 27 on histone H3 (H3K27ac), a mark associated with active enhancers[47] and promoters[48] (Extended Data Fig. 8a).

We found that just 15 min of drug addition increased Pol II Ser2 phos, further increasing over 1, 2 and 4 h, reflecting immediate transcriptional elongation, at well-characterized BCL6 target pro-apoptotic genes including *PMAIP1*, *FOXO3*, *BCL2L11* and *BCL6* itself (Fig. 4e,g,h and Extended Data Fig. 8b). Accompanying this immediate elongation effect was a loss of Pol II Ser5 phos, which could reflect a redistribution effect and/or a switch from pausing to productive elongation (Fig. 4e, middle row). Effects at downregulated genes were similar to those at unchanged genes and probably reflect background or a stress response. We further ascertained that BRD4 levels increase at the promoters of upregulated genes selectively, approximately 150% after just 1 h of TCIP1 addition (Fig. 4f, top row), consistent with its increase at BCL6-binding sites genome wide (Fig. 4d).

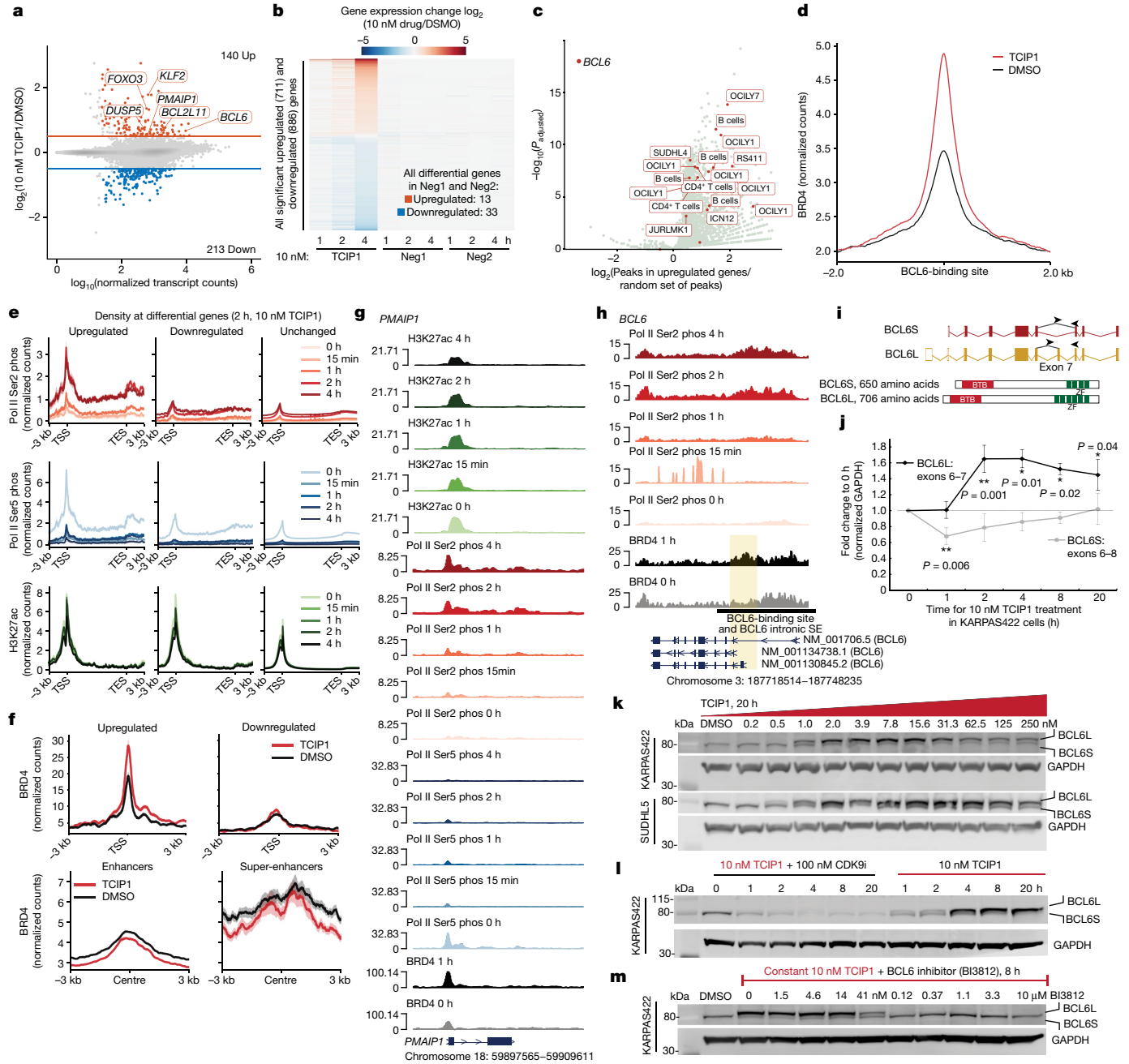

Fig. 4 | Rapid activation of BCL6 target genes by recruitment of BRD4. **a**, Gene expression changes after 10 nM TCIP1 for 2 h in KARPAS422, with well-known BCL6 targets labelled. *P* values were computed by a two-sided Wald test and adjusted for multiple comparisons by Benjamini–Hochberg. Differential gene cut-offs: $P_{adjusted} \leq 0.05$ and $|\log_2(\text{drug/DMSO})| \geq 0.5$; $n = 3$ biological replicates. **b**, Changes in gene expression after 1, 2 and 4 h of 10 nM TCIP1 compared with Neg1 and Neg2. **c**, Enrichment analysis of transcription factor binding in promoters of genes upregulated at 2 h after TCIP1 treatment in more than 4,500 public ChIP–seq datasets in blood-lineage cells. *P* values were computed by a two-sided Fisher's exact test and adjusted for multiple comparisons by Benjamini–Hochberg. **d**, BRD4 density in KARPAS422 cells at BCL6 summits after 1 h of 100 nM TCIP1. **e**, Time-dependent density of Pol II Ser2 phos, Pol II Ser5 phos and H3K27ac along gene bodies that are ±3 kb after 10 nM TCIP1, at differential genes identified by 2 h of RNA sequencing in **a**. TES, transcription end site; TSS, transcription start site. **f**, BRD4 density at differential genes, as in **e**, and enhancers and super-enhancers identified by H3K27ac (Methods). Metaprofiles and shading in **e** represent mean ± s.e. from spike-in-normalized and input-normalized ChIP–seq data, and in **f** represent mean ± s.e. from sequence-depth-normalized and input-normalized ChIP–seq data. **g**, ChIP–seq tracks at *PMAIP1* after addition of 10 nM TCIP1. **h**, Tracks at the *BCL6* locus, with alternative transcripts shown. SE, super-enhancer. Pol II Ser2 phos, Pol II Ser5 phos and H3K27ac tracks in **g**,**h** are spike-in- and input-normalized, and BRD4 tracks are sequence-depth- and input-normalized. **i**, Structures of BCL6 isoforms. ZF, zinc finger. **j**, mRNA of long and short isoforms of *BCL6* (BCL6L and BCL6S, respectively), measured by quantitative PCR with reverse transcription by primers specific to isoform-unique exon–exon junctions (shown by arrowheads in **i**). $n = 3$ biological replicates, mean ± s.d. *P* values were calculated by a two-tailed, unpaired Student's *t*-test. **k**, Induction of the BCL6L isoform by 1 nM or less TCIP1. **l**, Simultaneous treatment of 10 nM of TCIP1 and 100 nM of the CDK9 inhibitor (CDK9i) NVP2 to block elongation. **m**, Competitive titration of BI3812 against 10 nM TCIP1. The blots in **k**–**m** are representative of two biological replicates.

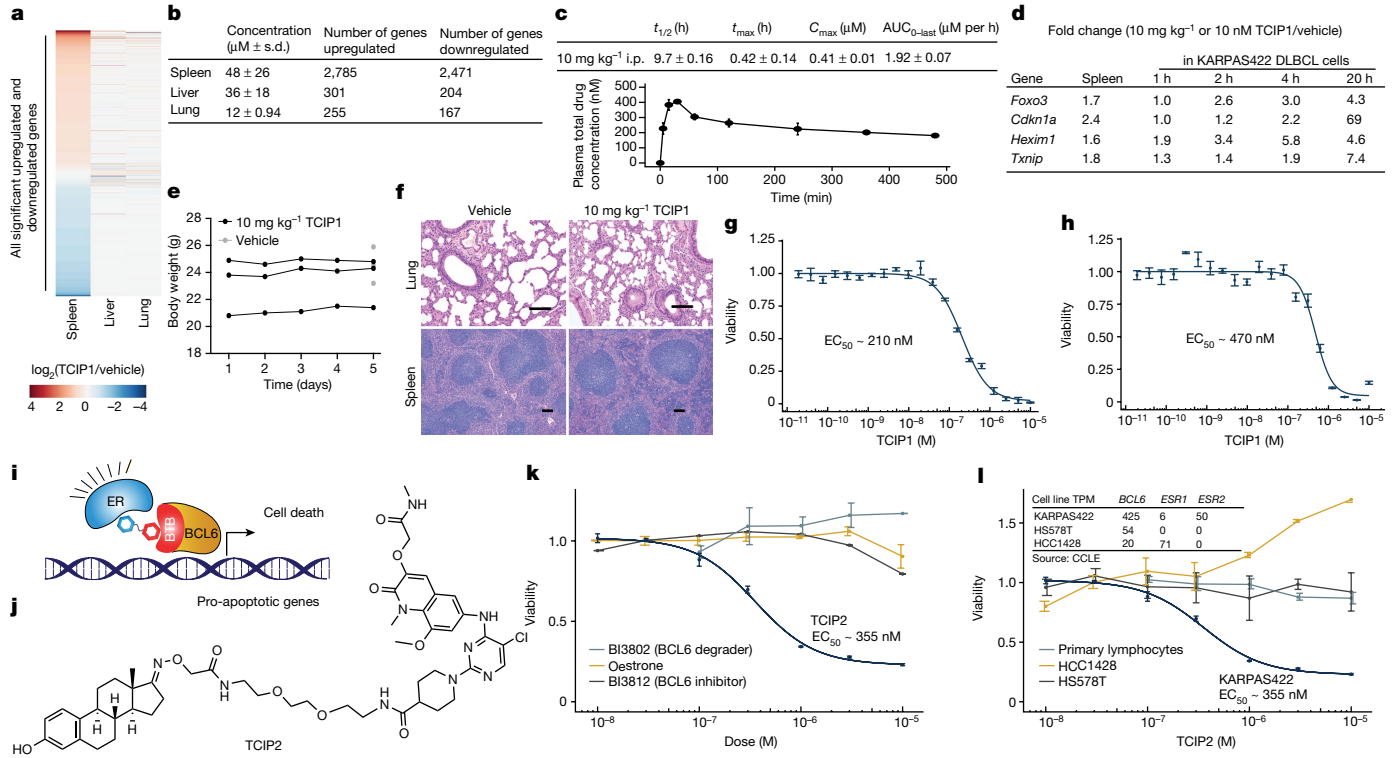

Fig. 5 | Toxicity of TCIP1 in mice and primary human cells and generalization to ER-positive cancers. a, Tissue-specific transcriptomic effects of TCIP1, treated at 10 mg kg^{-1} intraperitoneal (i.p.) once daily for 5 days. **b**, Quantification of transcriptome changes in the liver, lung and spleen and associated accumulated tissue concentrations of TCIP1. Treatment at 10 mg kg^{-1} TCIP1 intraperitoneal once daily, with measurement on day 5. $n = 3$ mice per treatment. **c**, Pharmacokinetic parameters of TCIP1. $t_{1/2}$, half-life; t_{max}, time to max serum concentration; C_{max}, maximum serum concentration; $AUC_{0\text{-last}}$, area under the curve from dosing to last measured concentration. **d**, Comparison of key gene targets upregulated by TCIP1 in both cultured DLBCL cells (KARPAS422) and in the spleen. **e**, Body weight of treated mice. No adverse effects or behavioural abnormalities were noticed. **f**, Haematoxylin and eosin staining of the lung and spleen from representative mice treated with vehicle and drug. Scale bars, 50 μm (lung images) and 100 μm (spleen images). $n = 3$ mice each for treatment and vehicle for **a**–**f**. **g**, Effect of TCIP1 on cell viability of primary human tonsillar lymphocytes. **h**, Effect of TCIP1 on cell viability of primary human fibroblasts. **i**, ER–BCL6 TCIP2 designed to induce cell death in oestrogen-positive, BCL6-overexpressing DLBCLs. **j**, Chemical structure of TCIP2. **k**, Effect on cell viability of TCIP2 compared with controls: oestrone, BI3812 (a BCL6(BTB) inhibitor) and BI3802 (a BCL6 degrader) in KARPAS422 cells with high ERβ (encoded by *ESR2*) levels. **l**, Measurement of the selective effect on cell viability by TCIP2 in DLBCL cells with coincident overexpression of ER and BCL6 (KARPAS422) compared with primary human lymphocytes, a triple-negative breast cancer cell line (HS578T) and ER-driven but BCL6-low breast cancer cells (HCC1428). CCLE, Cancer Cell Line Encyclopedia. $n = 3$ biological replicates, mean ± s.d. for **g**,**h**,**k**,**l**. Viability curves in **g**,**h**,**k**,**l** are after 72 h of drug treatment.

We used our H3K27ac ChIP–seq data to examine the consequences at regulatory regions such as active enhancers where there is a 20 times higher cumulative load of BRD4 than at other regions of the genome[49,50]. BRD4 occupancy decreased at enhancers approximately 10% 1 h after addition of TCIP1 (Fig. 4f, bottom row; example genome track of the OCA-B super-enhancer is shown in Extended Data Fig. 8e). In addition, there were negligible changes in H3K27ac either at promoters of differential genes (Fig. 4e) or genome wide; after 2 h, only 126 peaks increased, whereas 70 peaks decreased ($|\log_2(\text{TCIP1/DMSO})| \geq 0.5$, $P_{adjusted} \leq 0.05$) out of 51,678 total consensus peaks reconstructed (Extended Data Fig. 8c). This is consistent with the genetic studies of Melnick and colleagues, which point to a competition model between BCL6 and other transcription factors underlying repression[51]. Our data support a model in which TCIP1 borrows a fraction of the total BRD4, recruits it to BCL6-binding sites and BCL6-regulated genes, and rapidly activates transcriptional elongation and the expression of these target genes.

Rewiring the BCL6 autoinhibitory circuit

BCL6 expression is subject to negative autoregulation that originates from BCL6-binding sites in the first intron of the *BCL6* gene, which are often deleted or mutated in DLBCL[52,53], providing protection from cell death. The TCIPs that we have designed should convert this negative-feedback pathway to a positive-feedback pathway, by replacing the epigenetic repression that BCL6 provides[54], with transcriptional activation by BRD4. To determine whether this prediction is correct, we examined *BCL6* mRNA levels after treatment with TCIP1 and found that within 1–2 h of the addition of 10 nM TCIP1, the long isoform of BCL6 is upregulated at the expense of its short isoform due to transcription and alternative splicing of exon 7 in the *BCL6* gene (Fig. 4i,j). The BCL6 protein was significantly increased in a dose-dependent manner upon addition of TCIP1, also showing a hook effect, in two different DLBCL cell lines (Fig. 4k). Simultaneous addition of a nanomolar CDK9 inhibitor, NVP2 (ref. 45), to block elongation of transcription, prevented upregulation of BCL6 protein levels (Fig. 4l). The chemical controls Neg1 and Neg2 also did not affect BCL6 (Extended Data Fig. 9a). The kinetics of BCL6 induction were similar in two separate DLBCL cell lines (SUDHL5 and KARPAS422) (Extended Data Fig. 9c); in addition, BRD4 protein levels did not change substantially (Extended Data Fig. 9b).

Because the primary transcript of BCL6 is 24 kb and Pol II moves at 2–3 kb per minute, we hypothesized that transcription of *BCL6* must start almost immediately after addition of TCIP1. Indeed, in our ChIP–seq data, we observed that elongation of polymerase starts to increase

at exon–intron junctions at just 15 min, and continues to spread through the gene body at 1, 2 and 4 h after addition of 10 nM TCIP1 (Fig. 4h). BRD4 density increases modestly by 1 h at the known intronic BCL6-binding site. Finally, as in Fig. 3g, to clarify the role of ternary complex formation for the BCL6 upregulation observed, we titrated the BCL6(BTB) inhibitor BI3812 against a constant concentration of 10 nM TCIP1 and found that we could reverse the upregulation of BCL6 (Fig. 4m). Our data indicate that *BCL6* is itself a direct target of TCIP1 and TCIP1 can rewire its repressive negative-feedback pathway into a positive-feedback pathway, amplifying the potency of the molecule in killing cancer cells (model in Extended Data Fig. 9d).

Cell-type-specific activity of TCIP1

BCL6-knockout mice die of a complex inflammatory reaction that has been dissected to specific regions of the protein[55]. Because TCIP1 requires engagement of both BCL6 and BRD4, and also operates at a concentration that would occupy only a fraction of the total BCL6 molecules (unlike a degrader or inhibitor), we were curious about the potential toxicity of TCIP1. We evaluated the tolerability, pharmacokinetic properties and target engagement of TCIP1 in wild-type C57BL/6 mice treated for 5 days with 10 mg kg^{-1} TCIP1 once daily by intraperitoneal injection. TCIP1 induced dramatic transcriptomic changes in the spleen despite comparable tissue concentrations of drug (Fig. 5a,b). Serum concentrations were approximately 100–400-fold higher than expected therapeutic doses (Fig. 5c). Notable genes upregulated in DLBCL cells, such as *FOXO3*, were also upregulated in the spleen as well as other known BCL6 targets in lymphocytes (Fig. 5d and Supplementary Table 1). Despite the large transcriptomic changes in the spleen, TCIP1 was well tolerated with no adverse effects noticed and no significant changes in mouse body weight (Fig. 5e). Haematoxylin and eosin staining and examination (by H.V.) also did not reveal noticeable abnormalities such as inflammatory infiltrates or apoptotic cells (Fig. 5f). We also observed a 200–400-fold lower sensitivity in primary human fibroblasts (EC_{50} of approximately 470 nM) and lymphocytes (EC_{50} of approximately 210 nM) (Fig. 5g,h). T and B lymphocytes are particularly germane because they have among the highest levels of BCL6 (ref. 56). The data support the cellular evidence that TCIP1 acts in a context-specific manner dependent on coincident expression of BRD4 and BCL6.

Generality of the TCIP strategy

We explored the generality and predictability of the TCIP approach by designing and synthesizing a series of molecules predicted to borrow the transcriptional activity of the oestrogen hormone receptor protein to activate BCL6 target genes and produce cell death (Fig. 5i). We used the synthetic oestrogen, oestrone for these studies and constructed TCIP2 (Fig. 5j), which showed strong antiproliferative activity with an EC_{50} of 355 nM (Fig. 5k). As predicted, killing was most robust in DLBCL lines, such as KARPAS422, with higher expression of both ER and BCL6 (Fig. 5k). Several ER-positive human breast cancer cells with low levels of BCL6 showed enhanced proliferation, indicating that oestrone was active and that TCIPs are not intrinsically toxic in cells lacking BCL6 (Fig. 5l). By contrast, triple-negative breast cancer cell lines with neither detectable BCL6 nor ER were not affected by the ER–BCL6 TCIP2 (Fig. 5l). These studies suggest that other transcriptional activators could be predictably hijacked or rewired to facilitate transcription of pro-apoptotic genes in DLBCL cells.

Discussion

Existing approaches to targeted cancer chemotherapy rely on inhibiting or degrading a protein or preventing its synthesis by RNAi or CRISPR (or CRISPRi). These approaches require complete or near complete removal of the driver function, often resulting in mechanism-based toxicity when the cancer driver is an essential protein. However, by making use of the intrinsic driving pathways of the cancer cell and rewiring them to activate pathways of cell death, we have introduced an approach to cancer chemotherapy that is analogous to a dominant, gain-of-function mutation in genetics. TCIPs produce their effect by activating cell death signalling and rewiring only a fraction of the cancer driver molecules per cell to drive the phenotype. This assertion is supported by the fact that 10 nM TCIP1 produces only an approximately 1.5-fold increase in BRD4 at BCL6 sites over the genome and less than 10% loss at enhancers (Fig. 4d,f), despite robust gene activation and cell killing. A gain-of-function mechanism would also explain the far more robust cell killing seen with substantially lower concentrations of TCIP1 than the weaker antiproliferative effects of conventional small-molecule inhibitors or degraders of BCL6 (refs. 23,57,58) or BET proteins[24]. The wealth of regulators of programmed cell death suggests many opportunities to use diverse cancer drivers to generalize this strategy of killing cancer cells by rewiring the cancer driver circuitry.

Past studies have used CIPs of genetically modified transcription factors or epigenetic regulators to activate or repress signal transduction or transcription of exogenous or endogenous genes[9,12,14]. Small molecules that bind to DNA and/or nucleosomes have also been used for this purpose[13,59]. Although these studies were mechanistically informative and provided a catalogue of the biologic processes regulated by CIPs[15], they had little therapeutic potential because of the need to introduce genetically modified transcription factors or small molecules with relatively little genomic specificity. Our experiments developing TCIPs rely only on endogenous transcription factors and epigenetic modifiers with their intrinsic biologic specificity and capture the combinatorial use of transcriptional regulators. The activation of endogenous genes by small-molecule TCIPs might have application to many other areas of biology and medicine. For example, TCIPs could be designed for use in activating death pathways in senescent cells, activating the expression of therapeutic or haploinsufficient genes, activating the expression of neoantigens in human immunotherapy, or regulating gene expression in cells or organisms for synthetic biology applications.

Online content

Any methods, additional references, Nature Portfolio reporting summaries, source data, extended data, supplementary information, acknowledgements, peer review information; details of author contributions and competing interests; and statements of data and code availability are available at https://doi.org/10.1038/s41586-023-06348-2.

1. Weinberg, R. A. The action of oncogenes in the cytoplasm and nucleus. *Science* **230**, 770–776 (1985).
2. Davoli, T. et al. Cumulative haploinsufficiency and triplosensitivity drive aneuploidy patterns and shape the cancer genome. *Cell* **155**, 948–962 (2013).
3. Sanchez-Vega, F. et al. Oncogenic signaling pathways in The Cancer Genome Atlas. *Cell* **173**, 321–337.e10 (2018).
4. Denny, S. K. et al. Nfib promotes metastasis through a widespread increase in chromatin accessibility. *Cell* **166**, 328–342 (2016).
5. Hengartner, M. O. & Horvitz, H. R. *C. elegans* cell survival gene ced-9 encodes a functional homolog of the mammalian proto-oncogene bcl-2. *Cell* **76**, 665–676 (1994).
6. Strasser, A., O'Connor, L. & Dixit, V. M. Apoptosis signaling. *Annu. Rev. Biochem.* **69**, 217–245 (2000).
7. Schmitz, R. et al. Genetics and pathogenesis of diffuse large B-cell lymphoma. *N. Engl. J. Med.* **378**, 1396–1407 (2018).
8. Phan, R. T. & Dalla-Favera, R. The BCL6 proto-oncogene suppresses p53 expression in germinal-centre B cells. *Nature* **432**, 635–639 (2004).
9. Spencer, D. M., Wandless, T. J., Schreiber, S. L. & Crabtree, G. R. Controlling signal transduction with synthetic ligands. *Science* **262**, 1019–1024 (1993).
10. Spencer, D. M., Graef, I., Austin, D. J., Schreiber, S. L. & Crabtree, G. R. A general strategy for producing conditional alleles of Src-like tyrosine kinases. *Proc. Natl Acad. Sci. USA* **92**, 9805–9809 (1995).
11. Graef, I. A., Holsinger, L. J., Diver, S., Schreiber, S. L. & Crabtree, G. R. Proximity and orientation underlie signaling by the non-receptor tyrosine kinase ZAP70. *EMBO J.* **16**, 5618–5628 (1997).
12. Ho, S. N., Biggar, S. R., Spencer, D. M., Schreiber, S. L. & Crabtree, G. R. Dimeric ligands define a role for transcriptional activation domains in reinitiation. *Nature* **382**, 822–826 (1996).

13. Erwin, G. S. et al. Synthetic transcription elongation factors license transcription across repressive chromatin. *Science* **358**, 1617–1622 (2017).
14. Hathaway, N. A. et al. Dynamics and memory of heterochromatin in living cells. *Cell* **149**, 1447–1460 (2012).
15. Stanton, B. Z., Chory, E. J. & Crabtree, G. R. Chemically induced proximity in biology and medicine. *Science* https://doi.org/10.1126/science.aao5902 (2018).
16. Stanton, B. Z. et al. Smarca4 ATPase mutations disrupt direct eviction of PRC1 from chromatin. *Nat. Genet.* **49**, 282–288 (2017).
17. Burslem, G. M. & Crews, C. M. Proteolysis-targeting chimeras as therapeutics and tools for biological discovery. *Cell* **181**, 102–114 (2020).
18. Gestwicki, J. E., Crabtree, G. R. & Graef, I. A. Harnessing chaperones to generate small-molecule inhibitors of amyloid β aggregation. *Science* **306**, 865–869 (2004).
19. Freiberg, R. A. et al. Specific triggering of the Fas signal transduction pathway in normal human keratinocytes. *J. Biol. Chem.* **271**, 31666–31669 (1996).
20. MacCorkle, R. A., Freeman, K. W. & Spencer, D. M. Synthetic activation of caspases: artificial death switches. *Proc. Natl Acad. Sci. USA* **95**, 3655–3660 (1998).
21. Yang, X., Chang, H. Y. & Baltimore, D. Essential role of CED-4 oligomerization in CED-3 activation and apoptosis. *Science* **281**, 1355–1357 (1998).
22. Basso, K. et al. Integrated biochemical and computational approach identifies BCL6 direct target genes controlling multiple pathways in normal germinal center B cells. *Blood* **115**, 975–984 (2010).
23. Kerres, N. et al. Chemically induced degradation of the oncogenic transcription factor BCL6. *Cell Rep.* **20**, 2860–2875 (2017).
24. Filippakopoulos, P. et al. Selective inhibition of BET bromodomains. *Nature* **468**, 1067–1073 (2010).
25. Loven, J. et al. Selective inhibition of tumor oncogenes by disruption of super-enhancers. *Cell* **153**, 320–334 (2013).
26. Nagel, S. et al. Amplification at 11q23 targets protein kinase SIK2 in diffuse large B-cell lymphoma. *Leuk. Lymphoma* **51**, 881–891 (2010).
27. Dyer, M. J., Fischer, P., Nacheva, E., Labastide, W. & Karpas, A. A new human B-cell non-Hodgkin's lymphoma cell line (Karpas 422) exhibiting both t (14;18) and t(4;11) chromosomal translocations. *Blood* **75**, 709–714 (1990).
28. Shu, S. et al. Response and resistance to BET bromodomain inhibitors in triple-negative breast cancer. *Nature* **529**, 413–417 (2016).
29. Ghandi, M. et al. Next-generation characterization of the Cancer Cell Line Encyclopedia. *Nature* **569**, 503–508 (2019).
30. Yu, C. et al. High-throughput identification of genotype-specific cancer vulnerabilities in mixtures of barcoded tumor cell lines. *Nat. Biotechnol.* **34**, 419–423 (2016).
31. Winter, G. E. et al. Drug development. Phthalimide conjugation as a strategy for in vivo target protein degradation. *Science* **348**, 1376–1381 (2015).
32. Slabicki, M. et al. Small-molecule-induced polymerization triggers degradation of BCL6. *Nature* **588**, 164–168 (2020).
33. Nowak, R. P. et al. Plasticity in binding confers selectivity in ligand-induced protein degradation. *Nat. Chem. Biol.* **14**, 706–714 (2018).
34. Schultz, L. W. & Clardy, J. Chemical inducers of dimerization: the atomic structure of FKBP12-FK1012A-FKBP12. *Bioorg. Med. Chem. Lett.* **8**, 1–6 (1998).
35. Schreiber, S. L. The rise of molecular glues. *Cell* **184**, 3–9 (2021).
36. Barish, G. D. et al. Bcl-6 and NF-κB cistromes mediate opposing regulation of the innate immune response. *Genes Dev.* **24**, 2760–2765 (2010).
37. Perez-Rosado, A. et al. BCL6 represses NFκB activity in diffuse large B-cell lymphomas. *J. Pathol.* **214**, 498–507 (2008).
38. Brunet, A. et al. Akt promotes cell survival by phosphorylating and inhibiting a Forkhead transcription factor. *Cell* **96**, 857–868 (1999).
39. Hatzi, K. et al. A hybrid mechanism of action for BCL6 in B cells defined by formation of functionally distinct complexes at enhancers and promoters. *Cell Rep.* **4**, 578–588 (2013).
40. Renault, V. M. et al. The pro-longevity gene FoxO3 is a direct target of the p53 tumor suppressor. *Oncogene* **30**, 3207–3221 (2011).
41. Bradner, J. E., Hnisz, D. & Young, R. A. Transcriptional addiction in cancer. *Cell* **168**, 629–643 (2017).
42. Tsherniak, A. et al. Defining a cancer dependency map. *Cell* **170**, 564–576.e16 (2017).
43. Zou, Z., Ohta, T., Miura, F. & Oki, S. ChIP-Atlas 2021 update: a data-mining suite for exploring epigenomic landscapes by fully integrating ChIP-seq, ATAC-seq and Bisulfite-seq data. *Nucleic Acids Res.* https://doi.org/10.1093/nar/gkac199 (2022).
44. Hurtz, C. et al. Rationale for targeting BCL6 in MLL-rearranged acute lymphoblastic leukemia. *Genes Dev.* **33**, 1265–1279 (2019).
45. Winter, G. E. et al. BET bromodomain proteins function as master transcription elongation factors independent of CDK9 recruitment. *Mol. Cell* **67**, 5–18.e19 (2017).
46. Adelman, K. & Lis, J. T. Promoter-proximal pausing of RNA polymerase II: emerging roles in metazoans. *Nat. Rev. Genet.* **13**, 720–731 (2012).
47. Creyghton, M. P. et al. Histone H3K27ac separates active from poised enhancers and predicts developmental state. *Proc. Natl Acad. Sci. USA* **107**, 21931–21936 (2010).
48. Wang, Z. et al. Combinatorial patterns of histone acetylations and methylations in the human genome. *Nat. Genet.* **40**, 897–903 (2008).
49. Whyte, W. A. et al. Master transcription factors and mediator establish super-enhancers at key cell identity genes. *Cell* **153**, 307–319 (2013).
50. Hnisz, D. et al. Super-enhancers in the control of cell identity and disease. *Cell* **155**, 934–947 (2013).
51. Huang, C., Hatzi, K. & Melnick, A. Lineage-specific functions of Bcl-6 in immunity and inflammation are mediated by distinct biochemical mechanisms. *Nat. Immunol.* **14**, 380–388 (2013).
52. Wang, X., Li, Z., Naganuma, A. & Ye, B. H. Negative autoregulation of BCL-6 is bypassed by genetic alterations in diffuse large B cell lymphomas. *Proc. Natl Acad. Sci. USA* **99**, 15018–15023 (2002).
53. Pasqualucci, L. et al. Mutations of the BCL6 proto-oncogene disrupt its negative autoregulation in diffuse large B-cell lymphoma. *Blood* **101**, 2914–2923 (2003).
54. Gearhart, M. D., Corcoran, C. M., Wamstad, J. A. & Bardwell, V. J. Polycomb group and SCF ubiquitin ligases are found in a novel BCOR complex that is recruited to BCL6 targets. *Mol. Cell. Biol.* **26**, 6880–6889 (2006).
55. Huang, C. et al. The BCL6 RD2 domain governs commitment of activated B cells to form germinal centers. *Cell Rep.* **8**, 1497–1508 (2014).
56. Uhlen, M. et al. Proteomics. Tissue-based map of the human proteome. *Science* **347**, 1260419 (2015).
57. Davis, O. A. et al. Optimizing shape complementarity enables the discovery of potent tricyclic BCL6 inhibitors. *J. Med. Chem.* **65**, 8169–8190 (2022).
58. Bellenie, B. R. et al. Achieving in vivo target depletion through the discovery and optimization of benzimidazolone BCL6 degraders. *J. Med. Chem.* **63**, 4047–4068 (2020).
59. Ho, S. N., Boyer, S. H., Schreiber, S. L., Danishefsky, S. J. & Crabtree, G. R. Specific inhibition of formation of transcription complexes by a calicheamicin oligosaccharide: a paradigm for the development of transcriptional antagonists. *Proc. Natl Acad. Sci. USA* **91**, 9203–9207 (1994).

Methods

Cell culture

Lymphoma and leukaemia cells were cultured in RPMI-1640 (American Type Culture Collection (ATCC) 30-2001) + 10% FBS with antibiotics (100X PenStrep; 15140122, Gibco). Daudi cells were a gift from the laboratory of R. Levy (Stanford University) and originally from the ATCC. Raji cells were a gift from the laboratory of J. Cochran (Stanford University) and originally from the ATCC. Primary human tonsillar lymphocytes were a gift from M. M. Davis. Toldeo, K562, Reh and Pfeiffer cell lines were a gift from the laboratory of A. Alizadeh (Stanford University) and originally from the ATCC. KARPAS422 cells were obtained from Sigma (06101702). DOHH2 and OCILY19 were obtained from the DSMZ. All other cell lines (SUDHL5, HT, SUDHL10, DB, Jurkat and primary human fibroblasts) were obtained from the ATCC. Primary human fibroblasts were cultured in DMEM + 10% FBS with antibiotics and used at passages 3–5. Primary human tonsillar lymphocytes were a gift from M. M. Davis. Cells were routinely checked for mycoplasma and immediately checked upon suspicion. No cultures tested positive.

Cell viability measurements

Thirty thousand cells were plated in 100 µl media per well of a 96-well plate and treated with drug for indicated times and doses. A resazurin-based indicator of cell health (PrestoBlue; P50200, Thermo Fisher) was added for 1.5 h, after which the fluorescence ratio at 560/590 nm was recorded. The background fluorescence was subtracted and the signal was normalized to DMSO-treated cells. EC_{50} measurements on cell lines were done with four biological replicates by separate cell passages maintained by three independent investigators. Fit of dose–response curves to data and statistical analysis were performed using the drc package in R using the four-parameter log-logistic function.

PRISM cell proliferation assay

The PRISM cell proliferation assay was carried out as previously described[30]. In brief, up to 906 barcoded cell lines in pools of 20–25 were thawed and plated into 384-well plates (1,250 cells per well for adherent cells, 2,000 cells per well for suspension or mixed suspension–adherent pools). Cells were treated with an eight-point dose curve starting at 10 µM with threefold dilutions in triplicate and incubated for 120 h, then lysed. The barcode for each cell was read out by mRNA-based Luminex detection as previously described[60] and input to a standardized R pipeline (https://github.com/broadinstitute/prism_data_processing) to generate viability estimates relative to vehicle treatment and fit dose–response curves. The area under the dose–response curve (AUC), which is correlated with drug potency, was used as a metric of drug potency in a cell line, and correlated with *BCL6* transcripts per million as annotated in the Cancer Cell Line Encyclopedia[29].

Chemical synthesis

Additional details are provided in the Supplementary Methods.

Protein expression and purification

The construct for 6×His-TEV-BRD4(BD1) was described in Filippakopoulos, Qi et al.[24] and was a gift from N. Burgess-Brown (Addgene plasmid #38943; http://n2t.net/addgene:38943; RRID: Addgene_38943). The construct for BCL6(BTB)-AviTag, where the AviTag was later biotinylated in vitro using purified BirA, was based on previously designed BCL6 constructs used for TR-FRET assays, as reported in multiple papers including refs. 23,61 and contains amnio acids 5–129 with three mutations—C8Q, C67R and C84N—that enhance stability but have no difference on backbone structure with the wild-type version[62]. A Trx-6×His-HRV3C-BCL6(BTB) construct without the AviTag was produced similarly for isothermal calorimetry (ITC) studies where the Trx-6xHis tag was cleaved by addition of HRV3C. Additional details are provided in the Supplementary Methods.

TR-FRET

Each reaction contained 100 nM BRD4(BD1), 100 nM BCL6(BTB)-AviTag-Biot, 20 nM Streptavidin-FITC (SA1001, Thermo) and 1:400 anti-6×His terbium antibody (61HI2TLF, PerkinElmer) in 10 µl of buffer containing 20 mM HEPES, 150 mM NaCl, 0.1% BSA, 0.1% NP-40 and 1 mM TCEP in a 384-well plate. Protein was incubated with drug digitally dispensed (Tecan D300e) for 1 h in the dark at room temperature before excitation at 337 nm and measurement of emission at 520 nm (FITC) and 490 nm (terbium) with a PHERAstar FS plate reader (BMG Labtech). The ratio of signal at 520 nm to 490 nm was calculated and normalized to DMSO-treated conditions and plotted.

ITC

The tag-cleaved versions of BCL6(BTB) and BRD4(BD1) were used for experiments, in a VP-ITC machine. For binary assays with TCIP1, 400 µM BCL6(BTB) or BRD4(BD1) were titrated from the syringe into a cell containing 40 µM TCIP1. For the binary protein–protein ITC, 330 µM BCL6(BTB) was titrated into 68 µM BRD4(BD1). For binary assays with JQ1 or BI3812, 100 µM BCL6(BTB) or 350 µM BRD4(BD1) was titrated from the syringe into a cell containing 5 µM BI3812 or 20 µM JQ1. For the ternary complex assays, 200 µM BRD4(BD1) was incubated with 10 µM TCIP1 in the cell (20-fold excess, to drive saturation of the binary complex), and 100 µM BCL6(BTB) was titrated from the syringe, at 310 rpm stirring at 25 °C in a buffer containing 10 mM HEPES (pH 7.5), 200 mM NaCl, 5% glycerol, 1 mM TCEP and matched DMSO percent (never more than 0.4%) in the syringe and the cell. The first one or two injections and outliers from instrument noise were routinely excluded. Data were fit to a one-site model using MicroCal LLC Origin software.

Biolayer interferometry

The tag-cleaved version of BRD4(BD1) and biotinylated BCL6(BTB)-AviTag were used for experiments, in a Gator Bio BLI machine. Of BRD4(BD1), 50 µM was added to each well containing titrations of TCIP1 from 5.5 nM to 12 µM so that BRD4(BD1) would be in excess and drive binary BRD4(BD1)–TCIP1 complex formation. Of BCL6(BTB), 100 nM was loaded on the streptavidin tip. Experiments were carried out at 25 °C. After loading, association was carried out for 300 s, dissociation for 300 s and a baseline for 30 s. A TCIP1-only control was carried out for each concentration confirming that there was no binding between BCL6(BTB) and TCIP1 on its own. A BRD4(BD1)-only control was tested, similarly confirming that BCL6(BTB) and BRD4(BD1) do not interact on their own. Data were analysed in GraphPad Prism with the association curves fit to the model 'one-phase association' and the dissociation curves to the model 'one-phase decay' to obtain kinetic parameters. The K_d was obtained by fitting a 'one-site binding' curve to the span of each association curve versus the concentration of drug.

Flow cytometry

For annexin V assays, 500,000 cells plated at 1 M ml^{-1} and treated with drug for indicated timepoints and doses were harvested on ice and washed twice in 2.5% FBS/PBS. Of 7-AAD, 2.5 µl and 2.5 µl of FITC-annexin V (640922, BioLegend) were added. Cells were incubated for 15 min at room temperature, then immediately measured on a BD Accuri. Gates were drawn based on single-stain and no-stain controls. For cell cycle and TUNEL analysis, cells plated at 1 M ml^{-1} were treated with drug for indicated timepoints and doses and pulsed with 10 µM ethynyl-EdU (C10424, Thermo) for 2 h before harvesting on ice. One million cells were counted and washed in 2.5% FBS/PBS. Cells were resuspended at 10 M ml^{-1} and fixed in 4% paraformaldehyde, washed and permeabilized in 0.5% Triton X-100/PBS. Fixed and

permeabilized cells were washed and labelled with BrdUTP using terminal deoxynucleotidyl transferase (556405, BD) for 60 min at 37 °C, rinsed and then labelled with AlexaFluor 647-azide (C10424, Thermo) for 30 min at room temperature in the dark. After washes, the sample was incubated with 2 µl 7-AAD and 5 µl RNAseA for 30 min at room temperature in the dark, washed and measured on a BD Accuri. Gates were drawn based on single-stain and no-stain controls and kept constant across conditions.

BCL6 reporter assay

KARPAS422 cells were lentivirally transduced with a construct containing the reporter. After selection, cells were plated and treated with indicated amount of TCIP1 for 8 h. Cells were washed in 2.5% FBS/PBS, 1:250 v/v of 7-AAD was added to distinguish live from dead cells and harvested for flow cytometry on a BD Accuri. Given the polyclonal population after transduction, the area under the curve of the histogram representing the FITC signal across all live cells was calculated as an integrative measure of the total GFP signal. A GFP-positive gate was drawn off non-transduced cells and the area past the threshold for each sample was calculated and normalized to cells treated with DMSO.

The BCL6–BRD4 nanoBRET assay

HEK293T cells were transfected with 1 µg of a construct with an N-terminal fusion of HaloTag to full-length BCL6 and 1 µg of a construct with an N-terminal fusion of nanoLuc (nano-luciferase) to full-length BRD4 (N169A, Promega). A 12-point dose–response curve with three technical replicates for each TCIP was carried out, and corrected BRET ratios were calculated according to the manufacturer assay protocol (TM439, Promega). Data were fit using the R package drc using the four-parameter log-logistic function. EC_{50} values shown in Fig. 2g are 'left-side' EC_{50}, as curves displayed the characteristic hook effect of a bivalent molecule.

RNA extraction, qPCR and sequencing library preparation

Cells were plated at 1 M ml^{-1} and harvested in TRIsure (38033, Bioline). RNA was extracted using Direct-zol RNA MicroPrep columns (R2062, Zymo) treated with DNAseI. Complementary DNA (cDNA) was prepared for quantitative PCR with reverse transcription (RT–qPCR) using the SensiFAST cDNA preparation kit according to manufacturer instructions (65054, Bioline). Of cDNA, 1 µl was used per RT–qPCR prepared with SYBR Lo-ROX (94020, Bioline). For sequencing library preparation, polyA-containing transcripts were enriched for (E7490S, NEB) and prepared into paired-end libraries (E7760S, NEB). Libraries were sequenced on an Illumina NovaSeq (Novogene).

Western blots

Cells were plated at 1 M ml^{-1} and treated with drug at indicated timepoints and doses. Two million cells were harvested on ice in RIPA buffer (50 mM Tris-HCl (pH 8), 150 mM NaCl, 1% NP-40, 0.1% sodium deoxycholic acid salt (DOC), 1% SDS, protease inhibitor cocktail (homemade) and 1 mM DTT) and 1:200 benzonase (E1014, Sigma) was added and incubated for 20 min. After 10 min of centrifugation at 14,000*g* at 4 °C, the supernatant was collected and protein concentration was measured by Bradford. The antibodies used for immunoblots were: BCL6 (D65C10, Cell Signaling), BRD4 (ab243862, Abcam), BCL2 (15071, Cell Signaling), p53 (DO-1, Santa Cruz), MYC (D84C12, Cell Signaling), FOXO3 (75D8, Cell Signaling), p21 (12D1, Cell Signaling) and GAPDH (6C5, Santa Cruz). All antibodies were used at 1:1,000 v/v dilutions except GAPDH (1:2,000) and p21 (1:500). ImageStudio (LI-COR) was used for blot imaging.

RNA sequencing analysis

Raw reads were checked for quality using fastqc (https://www.bioinformatics.babraham.ac.uk/projects/fastqc/) and trimmed from adapters using cutadapt[63] using parameters cutadapt -a AGATCGGAAGAG CACACGTCTGAACTCCAGTCA -b AGATCGGAAGAGCGTCGTGTAGG GAAAGAGTGT --nextseq-trim=20 --minimum-length 1. Transcripts were quantified using kallisto[64] against the human Gencode v33 indexed transcriptome and annotations. Differential gene analysis was performed using DESeq2 (ref. 65) using apeglm[66] to shrink log_2 fold changes and pathway and enrichment analyses using Enrichr[67] and ChIP-Atlas[43]. For analysis of BCL6 binding at ±1 kb from the transcription start site of differentially regulated genes, BCL6 peaks were reconstructed from OCILY1 DLBCL cells as deposited in ref. 39, using macs2 (ref. 68) callpeak with a score cut-off 100 or more, and overlap was calculated.

ChIP–seq experiment and library preparation

Thirty million cells were treated with TCIP1 or DMSO for indicated timepoints. Cells were washed in PBS and crosslinked for 12 min in CiA Fix buffer (50 mM HEPES (pH 8.0), 1 mM EDTA, 0.5 mM EGTA and 100 mM NaCl) with the addition of formaldehyde to a final concentration of 1%. The crosslinking reaction was quenched by glycine added at 0.125 M final concentration. Crosslinked cells were centrifuged at 1,000*g* for 5 min. Nuclei were prepared by 10 min of incubation of resuspended pellet in CiA NP-Rinse 1 buffer (50 mM HEPES (pH 8.0), 140 mM NaCl, 1 mM EDTA, 10% glycerol, 0.5% IPEGAL CA-630 and 0.25% Triton X-100) followed by wash in CiA NP-Rinse 2 buffer (10 mM Tris (pH 8.0), 1 mM EDTA, 0.5 mM EGTA and 200 mM NaCl). The pellet was resuspended in CiA Covaris Shearing buffer (0.1% SDS, 1 mM EDTA (pH 8.0) and 10 mM Tris-HCl (pH 8.0)) with 1,000× protease inhibitors (Roche) and sonicated for 20 min with Covaris E220 sonicator (peak power of 140, duty factor of 5.0 and cycles/burst of 200). The distribution of fragments was confirmed with agarose gel. Of chromatin per ChIP, 300 µl was used with anti-BRD4 antibodies (E2A7X, Cell Signaling). Of chromatin, 50 µg was used with anti-Pol II Ser2 phos (ab5095, Abcam) and anti-Pol II Ser5 phos (3E8, ActiveMotif) antibodies. Of chromatin, 25 µg was used with anti-H3K27ac (ab4729, Abcam). For each Pol II Ser2 phos, Pol II Ser5 phos and H3K27ac ChIP, exactly 20 ng (for Pol II Ser2 phos and Pol II Ser5 phos) or 50 ng (for H3K27ac) *Drosophila* chromatin (53083, ActiveMotif) was spiked-in with 2 µl spike-in chromatin-specific antibody (61686, ActiveMotif). After overnight incubation at 4 °C in IP buffer (50 mM HEPES (pH 7.5), 300 mM NaCl, 1 mM EDTA, 1% Triton X-100, 0.1% DOC and 0.1% SDS), immunoprecipitates were washed twice with IP buffer, once with DOC buffer (10 mM Tris (pH 8), 0.25 M LiCl, 0.5% IPEGAL CA-630, 0.5% DOC and 1 mM EDTA) and once with 10 mM Tris/1 mM EDTA buffer (TE) pH 8. Immunoprecipitates and inputs were reverse crosslinked in TE/0.5% SDS/0.5 µg $µl^{-1}$ proteinase K for 55 °C for 3 h, then 65 °C for 18 h, and then DNA was purified using a PCR cleanup spin column (74609, Takara). The sequencing library preparation was performed using the NEBNext Ultra II DNA kit (E7645S). Libraries were sequenced on an Illumina NovaSeq (Novogene).

ChIP–seq analysis

The data quality was checked using fastqc. The raw reads were trimmed from adapters with trim_galore (parameters: --paired –illumina) and raw reads were aligned to the hg38 human genome assembly and the dm6 fly genome assembly using bowtie2 (parameters: --local --maxins 1000). Low-quality reads, duplicated reads and reads with multiple alignments were removed using SAMtools[69] and Picard (https://broadinstitute.github.io/picard/). macs2 (ref. 68) was used to map position of peaks with a false discovery rate cut-off of 0.05. Bedtools[70] was used to find a consensus set of peaks by merging peaks across multiple conditions (bedtools merge), to count the number of reads in peaks (bedtools intersect -c) and to generate genome coverage (bedtools genomecov -bga). deepTools[71] was used to generate coverage densities across multiple experimental conditions (deeptools computeMatrix and deeptools plotProfile) and to

generate bigwig files (deeptools bamCoverage), where reads mapping to ENCODE blacklist regions were excluded[72]. Normalization was performed as suggested by the manufacturer protocol (61686 and 53083, ActiveMotif) in which the human genome-mapped unique reads in each ChIP were downsampled proportional to a normalization factor calculated by: (1) counting the unique reads in each sample that align to the fly genome; (2) identifying the sample containing the least amount of mapped fly genome reads; and (3) computing the normalization factor for each sample as (reads mapping to the fly genome in the sample with minimum mapped fly reads)/(reads mapping to the fly genome in the current sample). This procedure was carried out on a per-antigen basis (that is, the H3K27ac ChIPs were treated separately from the Pol II Ser2 phos ChIPs, which were separate from the Poll II Ser5 phos ChIPs). The average percentage of reads in each sample that mapped to the fly genome was 1.8 ± 1.4% (mean ± s.d.). All browser tracks and metaprofiles shown were calculated with spike-in-normalized and input-subtracted data. The peak differential analysis and principal component analysis was performed using DESeq2 (ref. 65). The SRX4609168 public dataset was used to extract positions of BCL6 summits for Fig. 4d. Enhancers and super-enhancers used in Fig. 4f and Extended Data Fig. 8d,e were classified using the ROSE[49] algorithm by stitching together H3K27ac peaks in untreated cells within 12.5 kb but excluding regions within 2 kb of a transcription start site unless within a larger H3K27ac domain. Data from Bal et al.[73] were used to cross-check our analysis and annotate the BCL6 intronic hyper-mutated super-enhancer.

Mouse tolerability and pharmacokinetic study

The pharmacokinetic and tolerability study was performed in the Drug Metabolism and Pharmacokinetics (DMPK) Core facility at Scripps Florida (https://www.scripps.edu/science-and-medicine/cores-and-services/dmpk-core/index.html). Mice used were C57Bl/6J, male and 9 weeks old. Sex was not considered in the study design, no data were randomized and no experimenters were blinded. The mice were housed in individually ventilated cages in JAG 75 cages with micro-isolator lids. HEPA-filtered air was supplied into each cage at a rate of 60 air exchanges per hour for the mice. The dark–light cycle was set to 20:00 on and 20:00 off. The temperature was set at 72 °F and was maintained at ±2 °F. The humidity was low/Hi of 30–70%. There was a computerized system in place to control and or monitor the temperatures within the Animal Holding Room. Each animal room was equipped with a thermos-hygrometer that was monitored and recorded daily on the room log. Of TCIP1, 10 mg kg^{-1} was injected intraperitoneally into C57BL/6 male mice ($n = 3$ in treatment and $n = 3$ in vehicle conditions) using a 25–29-gauge needle to deliver 10 µl g^{-1} body weight of a formulation of 1 mg ml^{-1} TCIP1 in 5% DMSO, 5% Tween-80, and 90% saline. Vehicle was the same formulation (5%, 5% and 90% of DMSO, Tween-80 and saline, respectively). The formulation was checked to be a clear solution and after administration, the animal was put back in its cage. For pharmacokinetic properties, plasma levels were measured at 0, 5, 15, 30, 60, 120, 240, 360 and 480 min after drug administration. For tolerability work, body weights and observation of animal health were recorded each day through 5 days of dosing once daily. After 5 days, tissues were collected 8 h after the last drug administration and split into one part for RNA sequencing, homogenized in TRIzol (15596026, Thermo), another part for histology, snap-frozen, and another part for measurement of drug levels for which molar concentrations were recorded with the assumption of 1 g tissue was equal to 1 ml. Samples were processed for analysis by precipitation using acetonitrile and analysed with liquid chromatography–tandem mass spectrometry. Pharmacokinetic parameters were calculated using the noncompartmental analysis tool of WinNonlin Enterprise software (version 6.3). All procedures were approved by the Scripps Florida Institutional Animal Care and Use Committee, and the Scripps Vivarium is fully accredited by the Association for Assessment and Accreditation of Laboratory Animal Care International. Formalin-fixed paraffin-embedded blocks (on snap-frozen tissue) and haematoxylin and eosin staining were done by the Stanford Histology/Pathology Service Core by H.V. and P. Chu.

Reporting summary

Further information on research design is available in the Nature Portfolio Reporting Summary linked to this article.

Data availability

Uncropped blots of western blots and Coomassie gels of recombinant proteins are available in Supplementary Fig. 1a,b, respectively. The flow gating strategy is available in Supplementary Fig. 2. Select gene expression changes in tissue from mice treated with TCIP1 are annotated in Supplementary Table 1. Source data for mouse drug levels in plasma and tissue and for body weight changes are provided. Sequencing data have been deposited to GSE211282. Source data are provided with this paper.

60. Corsello, S. M. et al. Discovering the anti-cancer potential of non-oncology drugs by systematic viability profiling. *Nat. Cancer* **1**, 235–248 (2020).
61. McCoull, W. et al. Development of a novel B-cell lymphoma 6 (BCL6) PROTAC to provide insight into small molecule targeting of BCL6. *ACS Chem. Biol.* **13**, 3131–3141 (2018).
62. Stead, M. A. et al. Structure of the wild-type human BCL6 POZ domain. *Acta Crystallogr. Sect. F Struct. Biol. Cryst. Commun.* **64**, 1101–1104 (2008).
63. Martin, M. Cutadapt removes adapter sequences from high-throughput sequencing reads. *EMBnet.journal* **17**, 10 (2011).
64. Bray, N. L., Pimentel, H., Melsted, P. & Pachter, L. Near-optimal probabilistic RNA-seq quantification. *Nat. Biotechnol.* **34**, 525–527 (2016).
65. Love, M. I., Huber, W. & Anders, S. Moderated estimation of fold change and dispersion for RNA-seq data with DESeq2. *Genome Biol.* **15**, 550 (2014).
66. Zhu, A., Ibrahim, J. G. & Love, M. I. Heavy-tailed prior distributions for sequence count data: removing the noise and preserving large differences. *Bioinformatics* **35**, 2084–2092 (2019).
67. Chen, E. Y. et al. Enrichr: interactive and collaborative HTML5 gene list enrichment analysis tool. *BMC Bioinformatics* **14**, 128 (2013).
68. Zhang, Y. et al. Model-based analysis of ChIP-seq (MACS). *Genome Biol.* **9**, R137 (2008).
69. Li, H. et al. The Sequence Alignment/Map format and SAMtools. *Bioinformatics* **25**, 2078–2079 (2009).
70. Quinlan, A. R. & Hall, I. M. BEDTools: a flexible suite of utilities for comparing genomic features. *Bioinformatics* **26**, 841–842 (2010).
71. Ramírez, F. et al. deepTools2: a next generation web server for deep-sequencing data analysis. *Nucleic Acids Res.* **44**, W160–W165 (2016).
72. Amemiya, H. M., Kundaje, A. & Boyle, A. P. The ENCODE Blacklist: identification of problematic regions of the genome. *Sci. Rep.* https://doi.org/10.1038/s41598-019-45839-z (2019).
73. Bal, E. et al. Super-enhancer hypermutation alters oncogene expression in B cell lymphoma. *Nature* **607**, 808–815 (2022).

Acknowledgements The studies described in this article were funded from a grant from the HHMI to G.R.C. and NIH grants CA276167, CA163915 and MH126720-01 to G.R.C. Funding was also provided by a grant from the Mary Kay Foundation. Funding was provided to S.G. from the NIH grant 5F31HD103339-03. G.R.C., S.G., A.K., S.H.K., C.-Y.C. and J.M.S. were mentored and financially supported by Stanford's SPARK Translational Research Program. G.R.C. was supported by the David Korn Professorship. This research was financially supported by Stanford Bio-X. Funding was provided to N.S.G. from departmental funds from Chemical and Systems Biology and the Stanford Cancer Institute, and the Gray laboratory also receives or has received research funding from Novartis, Takeda, Astellas, Taiho, Jansen, Kinogen, Arbella, Deerfield, Springworks, Interline and Sanofi. Funding for pharmacokinetic studies was provided by NIH grant number 1 S10OD030332-01. M.R.G. is supported by a Leukemia and Lymphoma Society Scholar award. S.G. thanks T. Reindl, E. Bruguera and S. Hinshaw for helpful advice for the biochemical studies. We thank I. A. Graef for thoughtful comments on the manuscript, and members of the Crabtree and Gray laboratories for constructive comments.

Author contributions G.R.C. conceived the TCIP strategy to regulate endogenous genes and the rewiring of cancer drivers to activate cell death pathways. S.G. contributed many inventive ideas, designed the first effective TCIP and performed the biochemical, cell biological and genomic studies. A.K. contributed many inventive ideas, defined the conditions for TCIP use, carried out the first successful TCIP experiments and conducted the cell biological and genomic studies. C.-Y.C. suggested the use of BCL6 as a means of producing cell death. S.H.K. screened the cell death genes to detect those that would directly kill cancer cells. N.S.G. and S.G. designed the first effective TCIPs. X.L. synthesized the first effective TCIP. Z.L. and T.Z. contributed to TCIP design and optimization. W.J. synthesized TCIP1, the most potent TCIP to date. W.W. contributed innovative ideas to the computational analysis for the selection of TCIP components and helped fund the studies by writing grants with G.R.C. J.M.S. carried out experiments designed by G.R.C., S.G. and A.K. H.V. conducted the histopathology studies. H.Y. and M.R.G. contributed to TCIP1 application in DLBCL. The manuscript was written by G.R.C., S.G., A.K. and N.S.G. with input from all authors.

Competing interests G.R.C. is a founder and scientific advisor for Foghorn Therapeutics and Shenandoah Therapeutics. N.S.G. is a founder, science advisory board member (SAB) and equity holder in Syros, C4, Allorion, Lighthorse, Voronoi, Inception, Matchpoint, CobroVentures, GSK, Shenandoah (board member), Larkspur (board member) and Soltego (board member). The Gray laboratory receives or has received research funding from Novartis, Takeda, Astellas, Taiho, Jansen, Kinogen, Arbella, Deerfield, Springworks, Interline and Sanofi. T.Z. is a scientific founder, equity holder and consultant of Matchpoint, equity holder of Shenandoah, and consultant of Lighthorse. M.R.G. reports research funding from Sanofi, Kite/Gilead, Abbvie and Allogene; consulting for Abbvie, Allogene and Bristol Myers Squibb; honoraria from Tessa Therapeutics, Monte Rosa Therapeutics and Daiichi Sankyo; and stock ownership of KDAc Therapeutics. Shenandoah has a license from Stanford for the TCIP technology that was invented by G.R.C., S.G., A.K., C-Y.C, W.W., S.H.K., N.S.G., W.J., X.L. and Z.L. All other authors declare no competing interests.

Additional information

Supplementary information The online version contains supplementary material available at https://doi.org/10.1038/s41586-023-06348-2.

Correspondence and requests for materials should be addressed to Nathanael S. Gray or Gerald R. Crabtree.

Peer review information *Nature* thanks the anonymous reviewers for their contribution to the peer review of this work.